CHAPTER 2

LITERATURE REVIEW

2.1 Gold nanoparticles (AuNPs)

2.1.1 Introduction

AuNPs have been used in various field of study based on its unique properties and numerous surface functionality. Most researchers reported using spherical AuNPs (sAuNPs) as it has several advantageous properties such as, size and geometry-related optoelectronic properties, large surface-to-volume ratio, superb biocompatibility, and low toxicity as reported by Mintz et al. (2018), Satija et al. (2010) and Wulandari et al. (2015). Mintz et al. (2018) and Nagatani et al. (2006) also highlighted among the crucial physical properties of AuNPs is the surface plasmon resonance (SPR) and fluorescence quenching ability.

Influenced by the gold core size around 1 – 100 nm, AuNP exhibits a range of colour due to SPR that shown in the absorption peak ranging 500 – 550 nm (Figure 2.1).

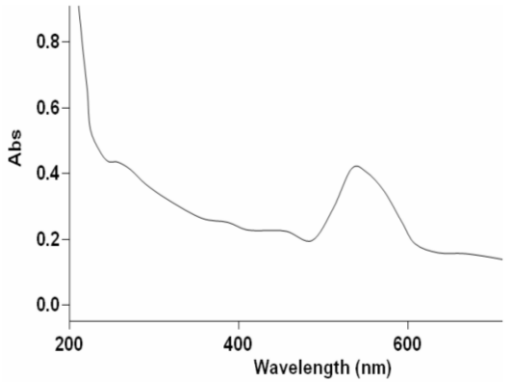

Figure 2.1: UV-Vis spectrum of gold nanoparticle with SPR band ranged in 500-550 nm (Honary et al. (2012))

The absorption peak that caused by the collective vibration of conduction electrons from the resonant excitation by the incoming photons is called surface plasmon band. Only AuNP with size larger than two nanometres can exhibit the surface plasmon band which is influenced by the gold geometry, solvent, surface ligands, charge, temperature, and interparticle space in the colloid (Louis and Pluchery, 2012; Satija et al.., 2010). The frequency of SPR absorption peak can be red-shifted through aggregation of AuNPs that also caused the broadening of the surface plasmon band and changing the colour of colloid from red to blue due to interparticle plasmon coupling (Louis & Pluchery, 2012).

Aside from SPR, AuNP also possesses the ability to quench fluorescence of nearby fluorophores by overlapping the fluorescence emission spectrum of the fluorophore with the surface plasmon band of AuNP. The quenching mechanism of AuNP is explained using Förster resonance energy transfer (FRET). FRET is a dynamic quenching mechanism that occurs when the fluorophore is in excited state due to the fact radiative and non-radiative decay of fluorophore are influenced by nanoparticles. In FRET, AuNP acts as an electron acceptor by charging and discharging the AuNP

through redox reaction between AuNP and the fluorophore (Cavalli et al., 2009; Mintz et al., 2018).

2.1.2 Synthesis of gold nanoparticle *via* trisodium citrate reduction

The basis of synthesizing AuNP as mentioned by Satija et al. (2010) is wet chemical method using any gold (III) salts and a reducing agent. The reducing agent was used to lower the oxidation state of the gold (III) salt to elemental gold with zero oxidation state. Trisodium citrate acts as a reducing agent to the gold (III) salt and a stabilizing agent to control the nanoparticle size growth. Uniquely, as Satija et al. (2010) mentioned, modifying the reaction parameters, including the reducing agent can affect the geometry of the AuNP, hence usage of trisodium citrate yielded spherical colloidal gold.

Synthesizing AuNP started way back when Turkevich et al. (1951) pioneered synthesizing monolayer colloidal gold with ten different methods using chloroauric acid ($HAuCl_4$) as the main precursor to form AuNP. Turkevich et al. (1951) reported the synthesized AuNP using trisodium citrate method was measured at 20 ± 1.5 nm. AuNP size also observed to be decreased as the reaction temperature and the concentration of trisodium citrate are decreased. However, the synthesis method reported having inconsistent deviation in the AuNP size ranging between 8.1 – 12.5% with particle size ranged between 15.1 – 21.5 nm.

Compared to the findings by Frens (1973), the refined trisodium citrate method yielded AuNP with 16 – 147 nm in size with decreasing mass of trisodium citrate used from 0.01 to 0.0016 g. Frens (1973) also mentioned the rate of reaction increases when the concentration of trisodium citrate was reduced while using the same parameters used

by Turkevich *et al.* (1951). Colours of the colloidal gold also ranged from orange to violet due to the changes in size of AuNP, mainly affecting AuNP with diameter size above 50 nm due to Willis-Tyndall scattering. Even though Frens (1973) synthesis method yield even coarser AuNP, the AuNP produced also irregular and quasi-spherical shaped nanoparticles, worsens with AuNP with size bigger than 40 nm.

Trisodium citrate method is then further fine-tuned by Grabar *et al.* (1995), modified the Turkevich et al. (1951) method with meticulous precautionary steps to eliminate the nucleation sites created by impurities on the surface of reaction vessel. Due to the necessary precautionary steps, AuNP produced was measured between 11.3 – 22.6 nm in size, smaller than aforementioned results.

In a more recent study, Xia et al. (2016) reinvigorate the Frens (1973) method by further refining the molar ratio of trisodium citrate to $HAuCl_4$ and introducing silver nitrate ($AgNO_3$) and tris(hydroxymethyl)aminomethane (Tris), as a secondary strong stabilizer. The optimum molar ratio of trisodium citrate to $HAuCl_4$ was kept at 4.1 while introducing $AgNO_3$ and Tris solution into the reaction mixture. $AgNO_3$ functioned to increase the redox reaction rate thus producing more Au^+ and acetone dicarboxylate at the early stage of reaction. Meanwhile, Tris solution provided amino groups to ensure more stable functionalized surface of colloidal gold and formed quasi-spherical AuNP with uniform sizes. With the improvement, the AuNPs produced possessed diameter of 1.8 – 362 nm.

2.1.3 Characteristics of gold nanoparticles

Typical method of validating the presence of AuNPs after the synthesis was using UV-Vis spectroscopy to observe the SPR band as aforementioned. Changes of

SPR band were used in different kinds of applications; namely determining the particle sizes and validating the changing of ligands on the surface of AuNPs. Haiss et al. (2007) and Tran et al. (2016) utilized the SPR banding changes to determine the resulting AuNPs sizes. Differing from method used by Tran et al. (2016), Haiss et al. (2007) quantitatively determined the particle sizes from the ratio of absorbance value at peak maxima of SPR band and absorbance value at 450 nm. SPR phenomenon also used as an indicator to validate the change of ligands on the surface of the nanoparticles. Rutherford et al. (2015) took this advantageous characteristic of AuNPs to verify the PEGylation of AuNPs was successfully done by comparing the UV-Vis spectra of both AuNPs before and after the PEGylation was done. This method of verifying the successful substitution of ligands also used by Durocher et al. (2009) and Dutse et al. (2017). Their works proved modifying the surface of AuNPs with other ligands could cause the UV-Vis spectra to be shifted.

In another research by Wulandari et al. (2015), citrate ion has been reported to be able to bind in different ways depending on the type of metal nanoparticles, in this case silver nanoparticles (AgNP) and AuNP. Citrate ion was found out to interact with AuNP and AgNP through monodentate bonding and ionic bonding, confirmed by Fourier Transform Infrared (FTIR) spectroscopy and molecular orbital (MO) calculations, respectively. Study of FTIR spectroscopy showed that carboxylate stretching bands of citrate ions modified when metal nanoparticles were stabilized, delineated in FTIR spectra. (Figure 2.2).

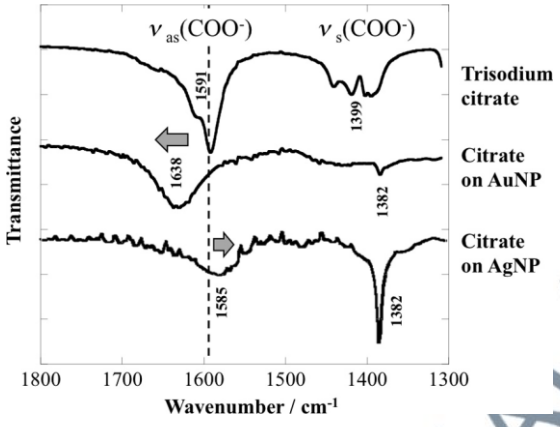

Figure 2.2: FTIR spectra of citrate ion on AuNP and AgNP, compared to trisodium citrate (Wulandari et al. (2015))

Figure 2.2 displays the citrate ion FTIR spectrum bound to AuNP and AgNP as the bulk product. Monodentate conformation of the citrate ion to AuNP resulted in a blue shifting of the carboxylate stretching band under plasmonic effect where the stretching of $\nu_s(COO^-)$ was equivalent to or less than the stretching of $\nu_{as}(COO^-)$. In Figure 2.3, the stretching of both bands on citrate ion bonded to AuNP's surface was identified.

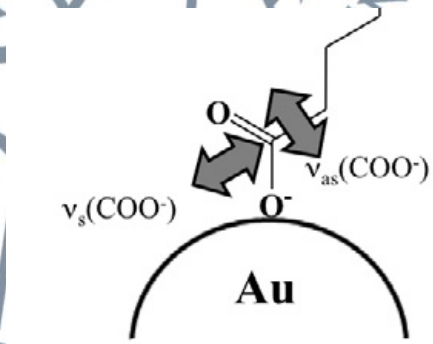

Figure 2.3: Schematics of carboxylate stretching bands on AuNP under plasmon effect (Wulandari et al. (2015))

Figure 2.3 displays the plasmon-effective carboxylate stretching bands of citrate ion on AuNP. The high frequency peak change from the FTIR spectra is attributed to

the asymmetric stretching vibration mode of citrate ion under the plasmonic effect influence which according to Wulandari et al. (2015) varies between metal salts and nanoparticles. According to Wulandari et al. (2015), the monodentate conformation of citrate ion to AuNP was verified by MO measurement, indicating the anchoring of only one oxygen atom from the carboxylate group in citrate ion to the AuNP surface.

Through this analysis, the discovery of citrate ion coordination on AuNP's surface empowers multiple researchers to use the citrate ion to produce assortments of their derivatives for various purposes, especially in chemical sensors and biosensors.

2.1.4 AuNPs as chemical sensors

Due to the increased ability of AuNPs to be used in the biomedical sector, the amount of research on the subject of AuNPs as a nanosensor has risen to date. Research conducted by Mintz et al. (2018) confirmed that energy transfer between AuNP and carbon dots allows α-L-fucosidase (AFU), the hepatocellular carcinoma tumour marker, to be identified. AFU's immunoassay in this study was based on the sandwich principle, a similar working concept of identification of HCG in commercially available pregnancy test devices, AuNP sandwiched AFU and carbon dots shown in Figure 2.4.

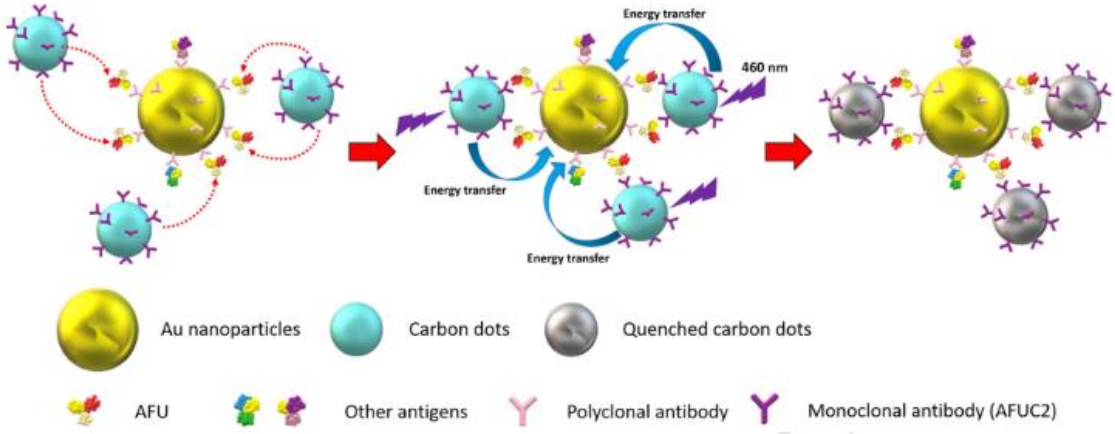

Figure 2.4: Simplified schematics of detection of AFU *via* AuNP and carbon dots (Mintz et al. (2018))

Figure 2.4 shown a condensed AFU identification schematics through AuNP and carbon dots. AuNP acted as a linking site to connect AFU molecules to polyclonal antibodies. Carbon dots functionalized with monoclonal antibody worked as a marker by changing colour due to carbon dot quenching by Förster resonance energy transfer. Photon emission at 480 nm produced colour of varying intensity related with the solution concentration of AFU. This was then used to determine the concentration of AFU in the blood serum sample as it had a strong linear relationship with the fluorescence produced by the carbon dot sample as claimed by Mintz et al. (2018).

In the meantime, reported cholera toxin in the United States of America can be identified by Khan et al. (2015) using a recently developed colorimetric and dynamic light scattering (DLS) assay based on AuNP. In this study, Khan et al. (2015) used mercaptopropionic acid (MPA) to modify the surface of AuNP produced. By linking agent known as N-(3-dimethylaminopropyl)-N'-ethylcarbodiimide hydrochloride (EDC HCl) and N-hydroxysulfosuccinimide, the cholera antibody was then conjugated to

MPA. Figure 2.5 shows the illustration used to detect cholera toxin on AuNP modification.

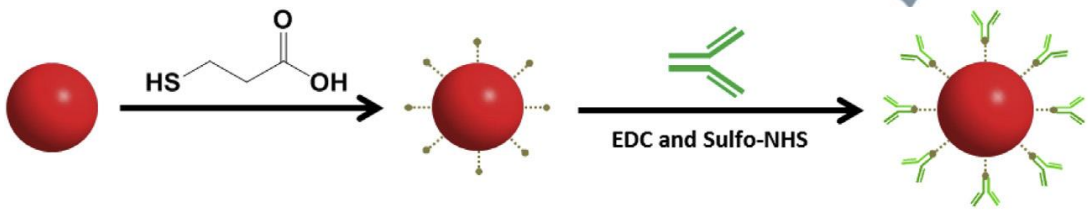

Figure 2.5: Schematics of modification of AuNP for cholera toxin sensing assay (Khan et al. (2015))

The altered AuNPs had monoclonal cholera antibody conjugated to the AuNP base, bound by MPA, referring to Figure 2.5. As stated by Khan et al. (2015), the monoclonal cholera antibody made the assay highly sensitive to cholera toxin. The colorimetric identification assay was focused on AuNP's shift in aggregation level, which triggered the colour change from burgundy to dark violet. The improvement in aggregation status was attributed to the unique identification of the cholera antibody monoclonal to the cholera poison B-subunit. However, one molecule of cholera poison can only be bonded with three antibody-functional AuNPs due to steric hindrance.

The use of AuNP can be rendered possible for the identification of tumour markers as stated by Gao et al. (2017), using appropriate unique antibodies for the tumour marker. Tumour markers can be identified using AuNP for antibody conjugation and gold deposition staining in the study conducted out by Gao et al. (2017). The tumour markers used in the work focused on carcinoembryonic antigen (CEA), cryokeratin 19 fragment antigen (CYFRA21-1), neuron-specific enolase (NSE) and dickkopf-1 (DKK-1). In order to detect the tumour markers, specific antibodies of each tumour marker

were combined with AuNP in a dilute polyethylene glycol solution suspended in a phosphate buffer solution. The assay setup consists of using AuNP with antibody-conjugated to bind to the tumour markers and using 2-(N-morpholino)ethanesulfonic acid, chloroauric acid and hydrogen peroxide as a staining solution for gold deposition to increase the visibility of AuNP bound to the target compound. It has been noted, according to Gao et al. (2017), the assay setup has achieved multiplexity as the AuNP can be used to identify all four tumour markers. Relative to widely used assay design by Clifton and Mountain (1997), it allowed lower sample amounts and shorter analytical duration. Since each AuNP was fortified with four distinct antibodies, AuNP's tumour marker binding rate was significantly higher than recorded by Gao et al. (2017), and Wu and Qu (2015) for typical biomarker detection assay. The sample design was also greatly improved by the gold deposition staining, which greatly contributed to the efficiency of identification.

2.2 Microfluidic paper-based analytical device (µPAD)

2.2.1 Introduction

µPAD is an expository tool designed to use liquid actions, high-precision control and manipulation to provide a robust, low-cost and easy-to-use medical diagnostics device that typically consist of a sequence of hydrophilic cellulose used to direct the liquid *via* imbibition from the inlet to the outlet.

In the plan point of view, there are four crucial regions of µPADs; inlet, channel, barrier, and outlet as displayed in Figure 2.6.

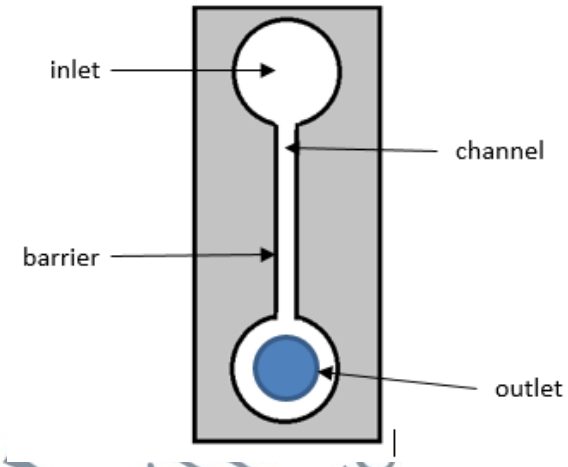

Figure 2.6: Regions in a microfluidic paper-based analytical device

The liquid sample is first dropped into the inlet, a hydrophilic area made up of cellulose substratum. The sample is then transferred via imbibition through the sub-millimeter hydrophilic channel to direct the liquid throughout the device. To avoid the sample from escaping the channel by diffusion, the channel is protected with a hydrophobic barrier typically from wax, hydrophobic or photoresist polymer,

dependent on the μPAD production techniques. Subsequently, a corresponding chemical or biochemical sensor placed in the outlet region for analytical purposes.

2.2.2 Applications of μPADs

μPADs are commonly used as a point-of-care test (POCT) in the medical field. POCT is also regarded as a bedside examination, described as a symptomatic clinical test done at the patient's time and area of treatment. This differs with conventional medical diagnostic work carried out to obtain the patient's history that requires the sample sent to the designated clinical laboratory to be analysed and taken a long time to complete. Therefore, it is progressively preferable to do POCT with μPADs as it is effective and delivers fast results as needed. For POCT, adaptability of μPADs is thriving as μPADs have been used to diagnose various ailments and disorders of the body, including tumour growth, blood glucose content, and pregnancy. Table 2.1 describes the utilizations of μPADs in medical field.

Table 2.1: Applications of μPADs in medical field (Shah et al. (2013))

Applications	Analytes	Platform	Detection method
General health diagnostics	Glucose, cholesterol, lactate	μPAD	CD, ECD, CLD
	Uric acid, ascorbic acid,	LFS	CD, ECD
	human chorionic gonadotropin	μPAD	CD, ECD, CLD
	Nitrile, ketones, ABO antigens, proteins (BSA)	μPAD	CD
	H-IgG, R-IgG, H-IgM	μPAD	CD
		LFS	CD, ECD
Cancer diagnostics	Prostate specific antigen,	μPAD	Electrochemiluminescence detection
	carcinoembryonic antigen, α-fetoprotein, circulating tumour cell, CA125, CA199	LFS	CD, ECD, CLD
Disease diagnostics	Phosphorylated acetylcholinesterase, human heart-type fatty acid-binding protein, genetic disease (nucleic acid	LFS	CD, ECD
	Nicotinamide adenine dinucleotide	μPAD	Electrochemiluminescence detection

CD: Colorimetric detection; ECD: Electrochemical detection; CLD: Chemiluminescence detection; H-IgG: Human IgG; H-IgM: Human IgM; LFS: Lateral flow strip; R-IgG: Rabbit IgG

Table 2.1 summed up the various uses of μPADs within the medical field in different sectors. Despite the fact that μPADs have been shown to be effective as a commonly used medical diagnostic device, μPADs themselves are expected to be developed as a large number of researchers constantly review μPAD's potential.

In addition to the use of μPAD as a point-of-care test in the medical field, the use of μPAD often applies to environmental monitoring as the output area of μPADs can provide colorimetric sensing site by using the correct sensor. The μPADs were used in a research conducted by Cate et al. (2014) to detect the presence of transition metals in welding fumes as an effort to reduce dangers and health risks for staff. There was a concern because the employees were not tested routinely for their susceptibility to the

particulate matter from the welding fumes. As indicated by Cate et al. (2014), routine checking and monitoring was conducted with a small representative of the workforce in order to reduce the expense and effort put into the monitoring, leaving the rest unchecked. As a result, a minimal-cost μPAD was developed to measure acid-extractable metals and confirmed independently using inductively coupled plasma-optical emission spectroscopy (ICP-OES) analysis. Cate et al. (2014) produced μPAD to quantify iron, copper, nickel and chromium levels by colorimetric analysis. Each of four metal forms was obtained from several small air sampling filter and isolated using microwave-assisted acid digestion, accompanied by neutralization before being loaded on the μPAD. Table 2.2 shows the results of the study of transition metals in observed welding fumes using the μPAD produced.

Table 2.2: Analysis results of transition metals present in welding fumes (Cate et al. (2014))

Analytes	Pre-treatment	Sensor	Linear response (μg)
Iron	1,10-phenanthroline	Reddish ferroin complex $[Fe(phen)_3]^{2+}$	1.1 – 10
Nickel	Acetic acid and sodium fluoride	Magenta complex with dimethylglyoxime	1 – 10
Copper	n/a	Bathocuproine	1.5 – 8
Chromium	Ceric (IV) ammonium nitrate and polydiallyldimethylammonium chloride	1,5-diphenylcarbazide and phthalic anhydride in acetone	0.15 – 6

n/a: not available

According to Cate et al. (2014), the direct response produced for iron was sufficient for occupational hazard exposure assessment as required by Occupational Safety and Health Administration (OSHA), but other transition metals were below the detection limit.

Numerous scientists have developed novelty compounds with expended selectivity and sensitivity, apart from using established chemicals as sensors for µPAD. Nanoparticles are among the highly sought-after compounds that are compatible with µPAD in this situation. In Thailand, the use of silver nanoparticles (AgNP) on µPAD was led by a group of researchers via colorimetric detection of copper (II) ion (Cu^{2+}). According to Ratnarathorn et al. (2012), the AgNP used has been altered by self-assembly of aminothiol compounds on the AgNP surface with homocysteine (Hcy) and dithreitol (DTT) and incubated at room temperature for two hours. The resultant AgNP from the modification of Hcy and DTT has a strong affinity to metal ions, shown by colour change after the addition of 7.8 nM of Cu^{2+} solution into the Hcy-DTT-AgNP mix, from yellow to orange attributable to catalytic oxidation of Hcy according to Smith and Reed (1992). The results of Ratnarathorn et al. (2012) were considered to be the first investigation utilizing nanosensor with µPAD, demonstrating the feasibility of using other sensors based on nanoparticles, particularly AuNP, as a sensor to be used on µPAD. Numerous studies adhered to the procedure and experimental method of Ratnarathorn et al. (2012) due to its simple to adapt to any materials.

Tseng et al. (2018) used a 3D-µPAD system to classify creatinine in the blood in another analysis using µPAD. In this study, the identification of creatinine was based on Jaffé reaction as shown in Figure 2.7.

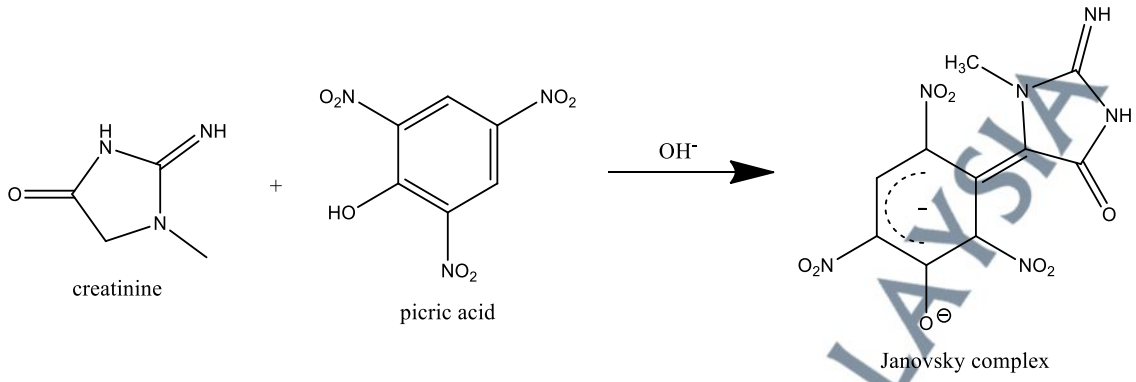

Figure 2.7: Jaffé reaction of creatinine and picric acid in alkaline medium (Randviir et al. (2013))

Figure 2.7 explains the Jaffé process, which involves Janovsky complex production from the creatinine and picric acid reaction. The generated Janovsky complex showed a different yellow-orange colour intensity that was linearly proportional to the amount of creatinine in the sample. Tseng et al. (2018) used a complementary metal oxide semiconductor (CMOS) camera to capture the image of the output area on the μPAD to evaluate the colour intensity of the generated Janovsky complex on the μPAD, then transferred the image via Wi-Fi using Arduino D1 Wi-Fi to a cell phone with customized application to calculate the creatinine concentration in the sample. Tseng et al. (2018) also featured the 3D-μPAD and the instrument produced was a significant improvement over previous creatinine detection by being flexible, prudent, small detection range fast analysis duration, lower sample size, and no pre-treatment and preparation required. Tseng et al. (2018) also included the effectiveness of the proposed creatinine detection system as serum tests and blood testing were associated with R^2 values of 0.9993 and 0.9920, respectively. The device was considered fit for medical application and point-of-care research with these tests.

2.3 Human chorionic gonadotropin

2.3.1 Introduction

Blood and urine as described by McPherson and Pincus (2017) are common sources of HCG screening in the field of identification of HCG. Essentially, HCG immunoassay used the concept of sandwich principle, where antibodies are labelled with HCG, i.e. enzyme or luminescent dye. The commonly available pregnancy test device incorporates the same mechanism on lateral flow strips as the system, based on the principle used. Otherwise known as a type of chromatographic immunoassay, urine testing was stated to have a detection limit of 1.2×10^{-3} – 6×10^{-3} ppm, but it differs significantly dependent on the brands of the test pack as mentioned by Vaitukaitis (2004). True findings can be obtained by using the first sample in the morning to assess conception in earlier stages using urine testing. Using the morning's most concentrated urine can further improve the test's quality. In the retrospect, it is not desirable to use watered down urine for test because the amount of HCG in the urine do not reflect the concentration of HCG in the blood. The test has lost its accuracy because of using diluted urine and may result in bogus outcomes. Another form of measurement of HCG is the serum test. The serum is isolated from venous blood and used approximately 2 – 4 ml of blood. Serum test consists of chemiluminescent or fluorometric immunoassay to recognize β-HCG subunit at 3×10^{-4} ppm. Serum test triumphs over serum test urine allows accurate quantification of HCG level.

2.3.2 Structure of HCG

Structural-wise, Cole (2015) described HCG as a large heterodimeric 237 amino acid glycoprotein, weighing at 36.7 kDa. HCG is a dimeric molecule as HCG consists of two subunits, α-HCG comparable to luteinizing hormone, follicle-stimulating hormone, and thyroid-stimulating hormone, whereas β-HCG is the HCG-specific main subunit. α-HCG has two side chains with N-linked oligosaccharides. Both side chains are connected to 52nd and 78th unit amino acid residues. Moreover, there are 145 amino acids in β-HCG. The β-subunit's huge structure is not held as a long chain but bound by bridges of disulfide. It also has two N-linked oligosaccharide side chains, bound to amino acid residues at the 13th and 30th positions, identical to its α-counterpart. β-HCG has four O-linked oligosaccharide units on the amino acid residue at 122nd to 145th, where the special serine-and proline-rich C-terminal extension is positioned. Figure 2.8 displays a 2D structure of HCG and metabolites.

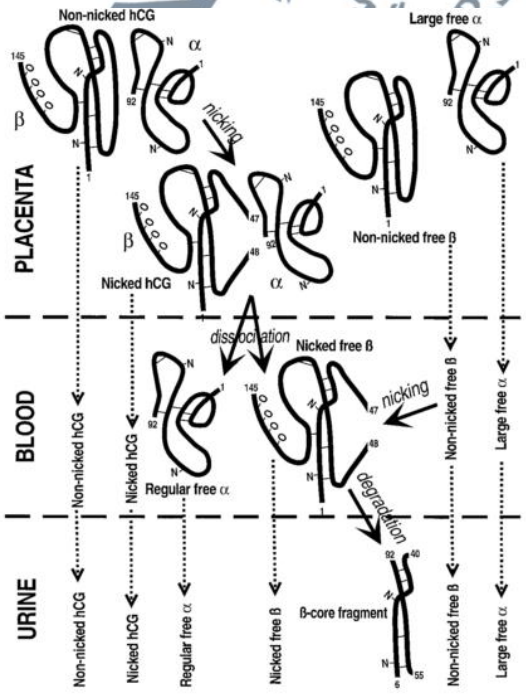

Figure 2.8: Representation of structures of HCG with its related subunits and metabolites in the placenta, blood, and urine (Cole (1997))

Figure 2.8 demonstrates the configurations of HCG in placenta, blood and urine with its associated subunits and metabolites. The dense lines are the chain of polypeptides, labelled to show the number of amino acids in the chain of polypeptides. The thin lines that cross the polypeptide chain are the molecule's disulfide bonds. Following amino acid configurations, subunit complexes folded, following the disulphide bonds within the subunits as per Lapthorn et al. (1994) and Morgan et al. (1975). HCG nicking, which exists only on the β-HCG, is focused on studies by Kardana et al. (1991), and the β-subunit structure is centered on Birken et al. (1988) study. On the polypeptide chain, N-and O-linked oligosaccharides are displayed by N and O respectively. Dotted arrows indicate the placenta, circulatory system, and urine that molecules flow into. The thick arrows indicate the β-HCG's nicking, dissociating and decaying course.

2.3.3 Applications in medical field

Apart from its use to assess pregnancy in women, according to the report by the American Cancer Society (2018), HCG was also pointed to as a tumour marker for various types of ailments. In females, HCG discharge is linked with gestational trophoblastic disease (GTD) diagnoses, including choriocarcinoma, mole hydatidiform, and tumour of germ cells. High level of HCG indicates physiological oddity in the female reproductive system, particularly if the woman is not pregnant. GTD confirmation diagnosis not only emphasizes the presence of HCG in the blood but also requires pelvic examination to be externally checked for any abnormal growth in the reproductive organ. Imaging diagnosis such as ultrasonography, x-ray scanning, computed tomography scan (CT scan), and magnetic resonance imaging (MRI) were used to monitor and track tumour growth during diagnosis and treatment itself. GTD treatment includes two options; surgery or chemotherapy. GTD treatment surgery may

be either dilation and curettage (D&C) procedure or tumour expulsion hysterectomy. Hysterectomy implies complete uterine extraction, which effectively sterilized the individual in return for thoroughly treated from GTD. However, D&C also makes it possible the patient to be pregnant as D&C removes only the endometrium wall with the tumour, and intravenously administers oxytocin to drain out of the residual tissues. Another approach for GTD, as stated by Tidy and Hancock (2010), is chemotherapy and radiotherapy, where chemotherapy requires medication intake, such as methotrexate and dactinomycin. The medications work to clear the detrimental cell that spread around the body. Radiotherapy also kills the cancer cell which utilizes nuclear radiation. During the follow-up and post-operation session, the attending medical staff will re-evaluate the level of HCG in the blood to ensure a decrease in the level of HCG in the blood.

Although men do not produce HCG as men should not be able to get pregnant, HCG was also produced alongside α-fetoprotein (AFP) from tumour cells of testicular cancer. Public classification of testicular cancer in two separate classes; seminoma and nonseminoma. Seminoma is a growth of tumours in all age groups, particularly in elderly people, and is less severe than nonseminoma. While, nonseminoma tumour is a tumour development that appears to arise in the early ages, propagate more rapidly, and occur in different tumour varieties. Testicular cancer diagnosed by identifying any lumps found by clinical examination, and ultrasonography aided in the visual identification of the tumour type. Treatment of testicular cancer typically requires surgery irrespective of whether the compromised testicle or retroperitoneal lymph node should also be extracted to avoid tumour spread. According to the National Cancer Institute (2018), radiotherapy is also used in the diagnosis of testicular cancer, which

uses high-energy, high-precision radiation from radioactive isotopes on tumour cells. Chemotherapy used as a subsequent treatment with prescribed medication to remove any moving cancer cell in the body. In any circumstance, radiotherapy and radiation are always be a risk of sterilization and accursed side effects. The key purpose of this study is therefore to achieve the combination of µPAD and AuNP-based HCG sensor to provide rapid identification of HCG apart from contributing to pregnancy monitoring and tumour detection.